Supplemental Figures

Supplemental Figure 1

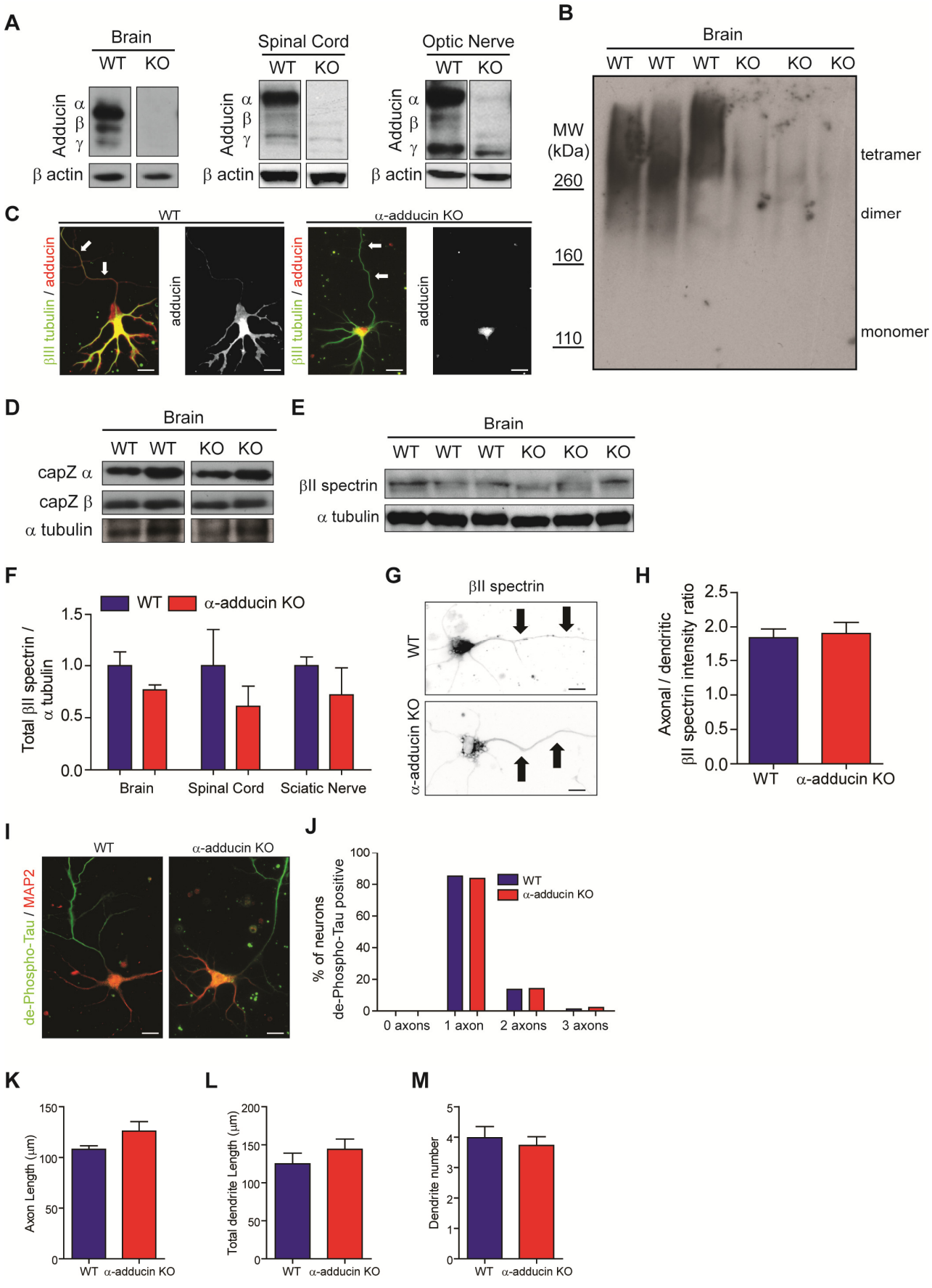

Supplemental Figure 1 (Related to Figure 1). α-adducin KO mice have severely decreased levels of β- and γ-adducin and lack functional adducin tetramers.

(A) Western blot analysis of brain, spinal cord and optic nerve of P30 WT and α-adducin KO mice using a pan-antibody that recognizes the α-, β- and γ-adducin forms (Xu et al., 2013).

(B) Anti-adducin western blot analysis of brain extracts of P30 WT and α-adducin KO brain extracts run on native gels. The 110, 160 and 260kDa standards are indicated together with the observed MW of adducin monomers (80-110 kDa), dimers (~200 kDa) (Gardner and Bennett, 1986) and tetramers (~320 kDa) (Hughes and Bennett, 1995).

(C) Anti-adducin immunofluorescence in E16 hippocampal neurons isolated from WT and α-adducin KO mice. Left panels: βIII-tubulin (green) and pan-adducin (red); right panels: pan-adducin (white). The axon is highlighted by white arrows. Scale bar: 10 µm.

(D) Western blot analysis of α and β capping protein (CapZ) and α tubulin in brain extracts of P30 WT and α-adducin KO mice.

(E) Western blot analysis of βII spectrin and α tubulin in brain extracts of P30 WT and α-adducin KO mice.

(F) Quantification of βII spectrin/α tubulin levels (as assessed by western blot) in brain, spinal cord and sciatic nerve samples.

(G) βII spectrin immunofluorescence in WT and α-adducin KO hippocampal neurons. Scale bar 10 µm.

(H) Ratio of the intensity of βII spectrin staining in the axon and dendrites.

(I); Anti-non-phosphorylated Tau (axonal marker, in green) and anti-MAP2 (dendritic marker, in red) immunofluorescence in WT and α-adducin KO DIV8 hippocampal neurons. Scale bar: 10 µm.

(J) Percentage of WT and α-adducin KO DIV3 hippocampal neurons with 0, 1, 2 and 3 neurites de-phopho-Tau positive.

(K-M) Axonal growth (K), dendritic outgrowth (L) and dendrite number (M) analysis in DIV3 WT and α-adducin KO hippocampal neurons. Graphs show mean ± s.e.m.

Supplemental Figure 2

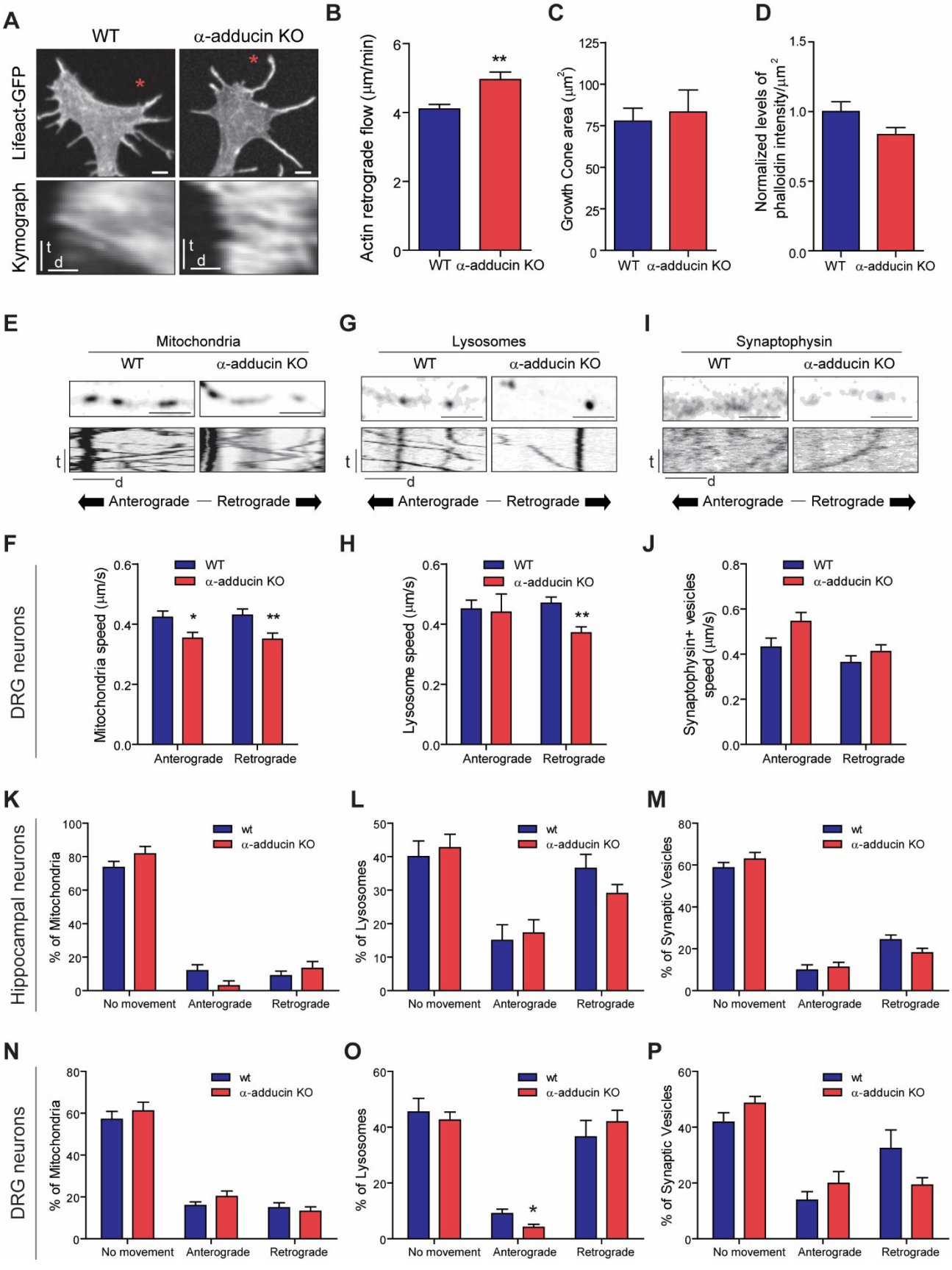

Supplemental Figure 2 (Related to Figure 2). In DRG neurons α-adducin KO mice have impaired cytoskeleton dynamics in the growth cone and decreased axonal transport of organelles.

(A) Representative growth cones of lifeAct-GFP transfected DRG neurons (upper) and respective kymographs (lower). Red asterisks highlight the region where kymographs were performed. Upper scale bar: 2 µm; Bottom: vertical scale bar: time (t)- 50 seconds, horizontal scale bar: distance (d)- 1 µm.

(B) Quantification of actin retrograde flow in DRG neurons from WT and α-adducin KO mice. ** $p<0.01$

(C) Growth cone area in DIV3 WT and α-adducin KO hippocampal neurons.

(D) Normalized levels of phalloidin intensity/μm^2 in DIV3 WT and α-adducin KO hippocampal neurons.

(E–J) Analysis in WT and α-adducin KO DRG neurons of the axonal transport of mitochondria (E and F), lysosomes (G and H) and synaptophysin (I and J); (E, G and I) Upper-still images at t=0; Lower- kymographs; Scale bar: time (t): 100 seconds; distance (d): 5 µm. (F, H and J) Quantification of the speed of axonal transport. Graphs show mean ± SEM. * $p<0.05$ and ** $p<0.01$.

(K–P) Analysis of the percentage of moving mitochondria (K, N), lysosomes (M, O) and synaptic vesicles (M, P) in hippocampal (K–M) and DRG neurons (N–P). * $p<0.05$.

Supplemental Experimental Procedures

Western blotting

For analyses under denaturing conditions, 10% SDS-PAGE gels or Criterion XT 3-8% gradient gels (Bio-rad), were run with brain, spinal cord or optic nerve extracts from at least n=3 WT and n=3 α-adducin KO P30 mice. Gels were transferred to nitrocellulose membranes for 2 hours using a semi-dry system. For analyses under native conditions, 4% PAGE gels were used with 50µg of brain extracts from WT (n=3) and α-adducin KO mice (n=3). Native gels were run and transferred to a PVDF membrane for 2 hours using a semi-dry system. Membranes were washed in Tris buffered saline (TBS) with 0.1% Tween-20, blocked in 5% non-fat dried milk in TBS for 1 hour at room temperature, and incubated with primary antibodies (in 5% BSA in TBS with 0.1% Tween-20) for 1 hour at room temperature or overnight at 4ºC. The following primary antibodies were used: rabbit anti-adducin, 1:1000 (Abcam, ab51130); mouse anti-β-actin, 1:5000 (Sigma, A5441); mouse anti-capping protein α1/2, 1:50 (Developmental Studies Hybridoma Bank, MAB 5B12.3); mouse anti-βII spectrin, 1:1000 (612562, BD Biosciences) and mouse anti-capping protein β2, 1:150 (Developmental Studies Hybridoma Bank, MAB 3F2.3). Membranes were washed and incubated with secondary antibodies in 5% non-fat dried milk in TBS with 0.1% Tween-20 for 1 hour, at room temperature. The secondary antibodies used were: donkey anti-mouse IgG, donkey anti-rat IgG or donkey anti-rabbit IgG conjugated with HRP, 1:5000 (all from Jackson Immunoresearch Europe). Membranes were then incubated for 5 minutes at room temperature with Luminata Crescendo Western HRP substrate (Millipore) and chemiluminescence was analyzed by either exposure to Amersham Hyperfilm ECL (GE healthcare) or detection in ChemiDoc XRS System (Bio-Rad).

Hippocampal neuron cultures

Hippocampal neuron cultures were performed as described (Kaech and Banker, 2006). Briefly, E16.5 embryos were individually dissected and genotyped. The hippocampus of each individual pup was digested 15 minutes in 0.06% porcine trypsin solution (Sigma, T4799), triturated, and plated either at 16000 cells/well in 24-well plates containing pre-coated glass cover slips treated with 20 µg/mL poly-L-lysine (Sigma, P2636), or at 12200 cells/well in 8-well µ-dishes (IBIDI, 80827) coated with 20 µg/mL poly-L-lysine for STED microscopy and axonal transport assays. Neurons were cultured in Neurobasal medium (Invitrogen) supplemented with 1x B27 (Gibco), 1% penicillin/streptomycin (Gibco) and 2 mM L-glutamine (Gibco). For neurite outgrowth and growth cone morphology assays, DIV3 hippocampal neurons were fixed in PHEM buffer (Flynn et al., 2012) and immunostained for βIII tubulin, 1:2000 (G7121, Promega) co-stained with rhodamine conjugated phalloidin 1:200 (R415, Lifesciences). To determine axon and dendrite length, the NeuronJ plug-in for ImageJ was used (Meijering et al., 2004) and 2 different litters were analyzed (n=3 for each genotype). For the analysis of the growth cone area and of F-actin intensity, measurements of the area occupied by rhodamine conjugated phalloidin (peripheral and transitional domain of the growth cone) were performed using Fiji software tools. Phalloidin intensity/μm^2 was quantified. Two different litters were analyzed (n=3 WT and n=4 α-adducin KO).

DRG neuron cultures

DRG neuron cultures were performed following the protocol detailed in (Fleming et al., 2009). Briefly, DRG from 8 weeks old Wistar rats were collected, digested for 90 minutes with 0.125% collagenase IV-S (Sigma, C1189), triturated and centrifuged in a 15% BSA gradient. For STED microscopy, 3750 cells/well were plated in 8-well µ-dishes coated with 20µg/mL poly-L-lysine (Sigma, P2636) and 5µg/mL laminin (Sigma, L2020) and grown in DMEM:F12 (Sigma, D8437) supplemented with 1x B27 (Gibco),

1% penicillin/streptomycin (Gibco), 2mM L-glutamine (Gibco) and 50ng/mL NGF (Millipore, 01-125).

Retina explant cultures

For retina explants, retinas from WT and α-adducin KO P2 mice were dissected in neurobasal medium and gently titrated with a P1000 tip. For STED microscopy, retina fragments were washed 3x with neurobasal medium and plated in 8-well µ-dishes (IBIDI, 80827) coated with 20 µg/mL poly-L-lysine (Sigma, P2636) and 2 µg/mL laminin (L2020, Sigma). Explants were incubated with complete retina explant growth media-Neurobasal (Invitrogen,) supplemented with 1x B27 (Gibco), 1% penicillin/streptomycin (Gibco), 0.2% fungizone (Gibco), 1 mM L-glutamine (Gibco), 5 ng/mL human recombinant BDNF (PeproTech) and 1 ng/mL CNTF (PrepoTech).

Morphometric analysis

For morphometric analyses, WT and α-adducin KO littermates were sacrificed at 3 different time points, P20 (n=4 WT; n=4 α-adducin KO), P60 (n=5 WT; n=5 α-adducin KO) and P100 (n=5 WT; n=4 α-adducin KO). Spinal cords, optic nerves and sciatic nerves were fixed for two weeks in 4% glutaraldehyde (Merck) in 0.1 M sodium cacodylate buffer (pH 7.4). After post-fixation with 1% OsO_4 in 0.1 M sodium cacodylate buffer (pH 7.4) for 2 hours, tissues were dehydrated and embedded in Epon (Electron Microscopy Sciences).

To determine axon caliber and density in the optic nerve and spinal cord, and unmyelinated axon density in sciatic nerve samples, ultrathin sections (60 nm) prepared in a Leica ultramicrotome were placed on 200-mesh copper grids (Electron Microscopy Sciences) and counterstained with alcoholic uranyl acetate solution (2% w/v; 10 minutes) and lead citrate (4% w/v; 10 minutes). Grids were observed in a JEOL JEM-1400 transmission electron microscope equipped with an Orious Sc1000 digital camera. Ten to 15 non-overlapping photomicrographs were obtained at 12000x (area

of each microphotograph was 165 μm^2) for optic nerve samples, and 5 non-overlapping images were obtained at 6000x (area of each microphotograph was 635 μm^2) for spinal cord samples, and used for determinations of axon density. For the analysis of axon diameter in the optic nerve, two 165μm^2 photomicrographs were used, with a minimum of 112 axons measured.

In sciatic nerves, to determine axon caliber and the density of myelinated axons, 1 µm-thick nerve sections were stained for 10 minutes with 1% p-phenylenediamine (PPD) in absolute methanol, dried, and mounted on a drop of DPX (Merck). The entire area of the nerve was photographed using an Olympus optical microscope equipped with an Olympus DP 25 camera and Cell B software, and images were imported into Photoshop (Adobe).

Actin retrograde flow and microtubule dynamics

DRG from WT and α-adducin KO P30 mice were nucleofected with either 0.75 µg Lifeact-GFP (Riedl et al., 2008) or 0.5 µg EB3-GFP (Stepanova et al., 2003), using the 4D Nucleofector Amaxa system (Lonza, CM#137 program), left in suspension in complete medium for 24h, and then plated 5700 cells/cm^2 in 20 µg/mL poly-L-lysine (Sigma) and 5 µg/mL laminin (Sigma) coated 35 mm µ-Dish (IBIDI, 81158). Hippocampal neurons were nucleofected with 0.75 µg Lifeact-GFP, using the 4D Nucleofector Amaxa system (Lonza, CU#133 program) and plated 70000 cells/cm^2 in 20 µg/mL poly-L-lysine (Sigma) coated 35 mm µ-Dish (Ibidi, 81158). Time-lapse recordings were performed in an Andor revolution XD spinning disk microscope (Andor Technologies) at 37ºC, at DIV2 for DRG neurons and DIV3 for hippocampal neurons. For the analysis of actin retrograde flow, neurons were imaged for 200 seconds (40 frames, captured each 5 seconds) and kymographs were generated with the Kymograph plug-in for ImageJ (DRG neurons: n=217 measurements from 40 WT growth cones; n=135 measurements from 27 α-adducin KO growth cones; hippocampal neurons: n=103 measurements from 14 WT growth cones; n=123

measurements from 15 α-adducin KO growth cones). For the analysis of microtubule dynamics, neurons were imaged for 200 seconds (100 frames, captured each 2 seconds) and kymographs were generated using a Matlab script (LAPSO) (Pereira and Maiato, 2010) (n=324 measurements from 13 WT growth cones; n=240 measurements from 14 α-adducin KO growth cones).

Axonal transport

Hippocampal and DRG neuron cultures were performed as detailed above. For the live imaging of axonal transport, DIV4 (DIV5 for synaptophysin) hippocampal neurons (a timepoint at which their polarized morphology allows the clear identification of the axon as the longest neurite) or DIV2 DRG neurons were used. Briefly neurons were incubated for 45 minutes with 100 nM of either Lysotracker (Life Technologies) or Mitotracker (Life Technologies) in complete medium. For synaptic vesicle analysis, DIV4 neurons were infected 24 hours with baculovirus expressing synaptophysin-GFP (Life Technologies). Transport of axonal mitochondria, lysosomes or synaptic vesicles was analyzed in a Leica SP5II confocal microscope (Leica Microsystems) with acquisition at 0.8 Hz for 2 min. Only vesicles and organelles moving for 10 consecutive frames were considered. In each case, at least 48 vesicles or organelles were measured per condition, from 15 axons; for DRG neurons, at least 114 vesicles or organelles were measured per condition from a minimum of 14 DRG neurons.

Immunofluorescence

Hippocampal neurons (DIV3 for anti-βII spectrin and non-phosphorylated Tau and DIV8 for anti-adducin, anti-non-phosphorylated Tau and anti-MAP2) were treated with 0.1% Triton-X, blocked and incubated with the following primary antibodies: rabbit anti-adducin 1:200 (Abcam, ab51130) and mouse anti βIII-tubulin 1:5000 (Promega, G7121); mouse anti-βII spectrin 1:125 (BD Biosciences, 612562) and rabbit anti-βIII-tubulin 1:2000 (Synaptic Systems, 302302); mouse anti-non-phosphorylated Tau 1:500

(Millipore, mab3420), rabbit anti-βIII-tubulin 1:2000 (Synaptic Systems, 302302) and chicken anti-MAP2 1:1000 (Aves Labs). Secondary antibodies used were donkey-anti-mouse Alexa Fluor 488, donkey-anti rabbit Alexa Fluor 568 and donkey-anti rabbit Alexa Fluor 647 all diluted 1:1000 (Invitrogen, A-21202, A10042 and A-31573 respectively) and goat anti-chicken Alexa Fluor 568 1:500 (Invitrogen, A-11040). Coverslips were mounted in fluoroshield (Sigma). In the case of adducin, non-phosphorylated Tau and MAP2 immunofluorescence, images were acquired in a Zeiss Imager Z1 at 63x. Neurons were scored for the number of non-phosphorylated Tau-positive processes (DIV3; WT n=81 cells and α-adducin KO n=92 cells). For spectrin immunofluorescence, images were acquired in a Leica DMI 6000B inverted microscope at 40x. The mean fluorescence intensity corresponding to βII spectrin labeling was measured in the axon and dendrites using Fiji software. The ratio of intensity of βII spectrin labeling in axons and dendrites was calculated (WT n=44 cells and α-adducin KO n=43 cells).

STED imaging of axonal actin rings

Fixed and SiR-actin stained axons were fine-tuned focused in their lateral outmost points and the focus point was confirmed by STED image sharpness. Raw STED images were deconvolved using Huygens Essential software (Scientific Volume Imaging B.V), using the adjusted GMLE algorithm. To analyze ring distribution, deconvolved images were plotted longitudinally in n=442 inter-ring spacings in rat DRG neurons (from 16 axons); n=952 WT (from 28 axons) and n=1100 α-adducin KO inter-ring spacings (from 32 axons) in DIV19 retina explants; and n=1011 WT (from 26 axons) and n=566 α-adducin KO inter-ring spacings (from 15 axons) in DIV8 hippocampal neurons; n=2305 WT (from 87 axons) and n=1909 α-adducin KO inter-ring spacings (from 59 axons) in DIV16 hippocampal neurons; n=1283 WT (from 37 axons) and n=1319 α-adducin KO inter-ring spacings (from 38 axons) in DIV30 hippocampal neurons. All measurements were performed using Huygens Software. To

determine axon diameter, the distance between the outer points (brighter, in the focus plane) that formed the actin ring was determined. Only actin rings unequivocally focused in the maximum wide plan were considered: n=1707 WT (from 28 axons) and n=1883 α-adducin KO (from 32 axons) in DIV19 retina explants; n=486 WT (from 21 axons) and n=547 α-adducin KO (from 13 axons) in DIV8 hippocampal neurons; n=2593 WT (from 59 axons) and n=2284 α-adducin KO (from 54 axons) in DIV16 hippocampal neurons; n=2173 WT (from 37 axons) and n=2321 α-adducin KO (from 38 axons) in DIV30 hippocampal neurons. For the measurement of F-actin density in individual actin rings, a measurement box was designed in each ring structure and the mean actin fluorescence/μm^2 was obtained using Fiji software. For each axon approximately 27 individual rings were measured and averaged (P8 WT axons n=24, P8 α-adducin KO axons n=12, P30 WT axons n=26 and P30 α-adducin KO axons n=26).

Supplemental References

Fleming, C.E., Mar, F.M., Franquinho, F., Saraiva, M.J., and Sousa, M.M. (2009). Transthyretin internalization by sensory neurons is megalin mediated and necessary for its neuritogenic activity. J Neurosci 29, 3220-3232.

Flynn, K.C., Hellal, F., Neukirchen, D., Jacob, S., Tahirovic, S., Dupraz, S., Stern, S., Garvalov, B.K., Gurniak, C., Shaw, A.E., et al. (2012). ADF/cofilin-mediated actin retrograde flow directs neurite formation in the developing brain. Neuron 76, 1091-1107.

Gardner, K., and Bennett, V. (1986). A new erythrocyte membrane-associated protein with calmodulin binding activity. Identification and purification. J Biol Chem 261, 1339-1348.

Hughes, C.A., and Bennett, V. (1995). Adducin: a physical model with implications for function in assembly of spectrin-actin complexes. J Biol Chem 270, 18990-18996.

Kaech, S., and Banker, G. (2006). Culturing hippocampal neurons. Nat Protoc 1, 2406-2415.

Meijering, E., Jacob, M., Sarria, J.C., Steiner, P., Hirling, H., and Unser, M. (2004). Design and validation of a tool for neurite tracing and analysis in fluorescence microscopy images. Cytometry A 58, 167-176.

Pereira, A.J., and Maiato, H. (2010). Improved kymography tools and its applications to mitosis. Methods 51, 214-219.

Riedl, J., Crevenna, A.H., Kessenbrock, K., Yu, J.H., Neukirchen, D., Bista, M., Bradke, F., Jenne, D., Holak, T.A., Werb, Z., et al. (2008). Lifeact: a versatile marker to visualize F-actin. Nat Methods 5, 605-607.

Stepanova, T., Slemmer, J., Hoogenraad, C.C., Lansbergen, G., Dortland, B., De Zeeuw, C.I., Grosveld, F., van Cappellen, G., Akhmanova, A., and Galjart, N. (2003). Visualization of microtubule growth in cultured neurons via the use of EB3-GFP (end-binding protein 3-green fluorescent protein). J Neurosci 23, 2655-2664.

Xu, K., Zhong, G., and Zhuang, X. (2013). Actin, spectrin, and associated proteins form a periodic cytoskeletal structure in axons. Science 339, 452-456.